ISSN 1810-2328, Journal of Engineering Thermophysics, 2021, Vol. 30, No. 2, pp. 300–316. © Pleiades Publishing, Ltd., 2021.

Investigation of Graphene Oxide-Distilled Water Nanofluids with Consideration of Heat Transfer and Flow Structure for Backward-Facing Step Flow

K. Karabulut[1]* and D. E. Alnak[2]**

[1] *Sivas Cumhuriyet University, Sivas Technical Sciences Vocational High School, Electric and Energy Department, Sivas, 58140 Turkey*

[2] *Sivas Cumhuriyet University, Technology Faculty, Automotive Engineering Department, Sivas, 58140 Turkey*

Received November 3, 2020; in final form, April 22, 2021; accepted April 30, 2021

Abstract—The backward-facing step flow is seen in applications in our daily life: the high attack angle at airfoil, the separation flow behind a vehicle, the flow in a gas turbine, and the flow around a boat or building. In view of increasing the heat and mass transfer, control of the backward step region is important. In this study, the heat transfer and flow structures with turbulence of step corner structures with a chamfer h/2 and h long and without chamfer were numerically examined with GO (Graphene Oxide)-distilled water (DW) solutions of volumetric concentrations of 0.01% and 0.02% in comparison with distilled water in a vertically positioned backward-facing step flow geometry. The results of the study were obtained via solving conservation equations of a three dimensional and steady k-ε turbulence model with the Boussinesq approach using the ANSYS-FLUENT-18.0 computer program. The nanofluids used in the study were considered as single-phase ones, and experimentally obtained thermophysical values were used. The study was carried out for Reynolds numbers of 5000 and 7500. The findings of present study were compared with the numerical results of a work found in the literature. The outcomes were found to be compatible and acceptable. The results were presented as variations of the Nu number, fluid temperature, turbulence kinetic energy, and pressure. In addition, the contours of the temperature and velocity and streamline distributions were visualized for a backward-facing step flow geometry. For Re = 7500 and the step geometry with an h-long chamfer, the average Nu number values for the 0.01% and 0.02% GO-DW nanofluids were determined to be higher by 11.7% and 14.33%, respectively, than those for distilled water.

DOI: 10.1134/S1810232821020119

1. INTRODUCTION

A backward-facing step flow, which is a separated flow model, is encountered in many engineering applications. A separation flow behind a vehicle, inside a condenser/burner or inlet tunnel flow of an engine, airfoil flow at a large attack angle, spoiler flows, and flows around a boat or building are examples of backward-facing step flow.

The thermal performance of systems such as heat exchangers, solar heaters, nuclear reactors, coolers, and hydrogen storage units used in energy conversion applications mainly depends on the thermophysical properties of conventional heat transfer fluids such as water, ethylene glycol, and oil. However, water, oils, and glycols exhibit poor heat transfer performance because of their low thermal conductivity. Today, research and development studies are carried out to improve the heat transfer properties of fluids in this direction. In addition, since solid materials have higher thermal conductivity values as compared with liquids, solid particles added to a liquid increase the thermal conductivity and heat transfer performance of the (base) fluid [1].

*E-mails: kkarabulut@cumhuriyet.edu.tr
**E-mail: dealnak@cumhuriyet.edu.tr

At first, micrometer- or even millimeter-sized solid particles were mixed into base fluids to form a suspension. These solid particles, which are large-sized as compared with nanoparticles, cause some undesirable consequences in practice, such as abrasion of pipelines, blockages in micro channels, and pressure drop increase. The large size of the particles and the difficulties experienced with smaller size particles during the production phase were factors limiting the application. However, initially only mixtures in the form of liquid suspension, which were of theoretical interest, were found to show promising effects in experimental studies. For this reason, there appeared an idea of adding solid particles to conventional heat transfer fluids, which was initiated in 1881 under the leadership of Maxwell, to increase the thermal conductivity [2, 3]. Since improvements in the properties of these fluids are of critical importance, research on innovative working fluids referred to as nanofluids has recently become the focus of attention [4, 5]. Nanofluids consist of particles of 100 nm and smaller in size, such as metal oxides, metals, single- and multi-layer carbon nanotubes, graphite, graphene, and graphene oxide, and generally are added to Newtonian fluids in low concentrations. While nanofluids improve thermophysical properties such as thermal diffusion and thermal conductivity, they provide excellent stability and convection heat transfer coefficient values and slightly increase the pressure drop and pumping power as compared with the base fluid [6, 7]. Since the idea of obtaining new fluids by adding nanoparticles to conventional fluids is expected to enhance the fluid thermal performance due to improvement in the thermal conductivity, it is reasonable to conduct intensive research on nanofluids. As compared with metals and metal oxides, carbon-based materials are of greater interest because they have high thermal conductivity and low density [8].

Graphene is a two dimensional one-atom-thick hexagonal structure formed by different arrangements of carbon atoms in one plane. Owing to this structure, graphene has outstanding mechanical, thermal, and electrical properties and has become a focus of interest for many researchers [9]. Graphene has very good heat transfer performance; the thermal conductivity of a single-layer graphene nanoparticle is 5000 W/m K at room temperature; the area of the surface is 2630 m^2/g [10]. When graphite is oxidized to GO, its thermal conductivity becomes lower. Because the GO has a water-like property, the stability of the nanofluid used increases and no sedimentation occurs [11].

In recent years, various working fluids have been studied in backward-facing step flows as prototypes for separation and recombination flows. Armaly et al. [12] changed the flow type by increasing the Re number at the inlet in their experiments carried out with air. They found the recombination point to depend on this general parameter and essentially vary among laminar, transition, and turbulent flows. Besides, for a sufficiently large Re number and a fully developed turbulent flow, the recombination point is independent of the Re number. Nadge and Govardhan [13] studied the influence of general parameters such as the Re number and step height on the shape of the recirculation region and showed this region to remain completely unchanged throughout the examined variable range if the recombination length and step height are dimensionless. Kasagi and Matsunaga [14] measured triple correlations and turbulent kinetic energy masses in a fully developed turbulent backward-facing step flow. Le et al. examined the interaction of turbulence motions in detail in one of their numerical studies [15]. With their high-resolution data, the wall shear rate and Reynolds stress masses, which are very difficult to measure in experiments, could be calculated. However, in a settlement that varies greatly over time, a sudden recombination of fully developed turbulent flow occurs. This topic has encouraged some researchers to reconnect up to a certain percentage of advanced fluid flow [16].

Heat transfer studies in backward-facing step flows are still very few. In an experimental study by Vogel and Eaton [17], turbulent heat transfer in air was investigated as a common benchmark. The research showed that the classical Re comparison did not maintain the average flow, but the fluctuating values were particularly high in the recombination region. The Reynolds number comparison assumes that the heat transfer in the wall is proportional to the shear in the wall. Keating et al. [18] successfully studied this situation numerically and identified turbulent structures affecting the heat transfer near the wall. Another situation of turbulent heat transfer behind a step was investigated numerically by Avancha and Pletcher [19], who considered a situation where air was used as a means of transport. Both numerical studies showed that Reynolds number similarity did not maintain the recombination region.

In this study, unlike the studies found in the literature, both turbulent heat transfer and flow properties were numerically examined with nanofluids for an h/2- and h-long chamfer in the step corner in vertically-located backward-facing step flow geometries for Reynolds numbers of 5000 and 7500. One of the walls behind the backward-facing step was kept at a constant temperature, while the others

were adiabatic. GO-DW nanofluids, which have superior heat transfer properties, with volumetric concentrations of 0.01% and 0.02% and DW were used as working fluids. The nanofluids used in the study were considered as single-phase, and experimentally obtained thermophysical values were employed. The fluid temperature at the inlet to the channel was 303 K, while that of the wall behind the backward-facing step was 316.5 K. The expansion rate of the backward-facing step was 1.5. As seen in the literature, in practical work with liquid fluids, it is important to consider the lifting effects especially if the vertical temperature difference is large. For this reason, in this study, the lifting effects were taken into consideration via the Boussinesq approach. The findings of the study resulted from solving three-dimensional steady conservation equations using the ANSYS-FLUENT-18.0 computer program with a k-ε turbulence model with the Boussinesq approach. The presented study was compared with numerical results in the literature, and they were found to be compatible and acceptable. The results have been presented as the Nu number, fluid temperature, turbulence kinetic energy, and pressure variations. In addition, the temperature, velocity, and streamline distributions in backward-facing step flow geometries were visualized.

2. NUMERICAL METHOD

The numerical study was performed by solving three-dimensional steady continuity, momentum, and energy equations using a computer program based on the ANSYS-FLUENT-18.0 finite volume method. In the study, while the k-ε model was used as the turbulence model, the Boussinesq approach took the lifting effects into consideration.

Convergence of calculations for continuity and momentum equations was stopped when the convergence scale was less than 10^{-6}; this value was 10^{-7} for the energy equation. A second order upwind scheme was implemented for solving the momentum and energy terms. Similarly, the pressure terms were solved using standard methods; the pressure and velocity coupling was solved using the SIMPLE method. A tetrahedral mesh structure was used for simulation.

The flow and heat transfers through the geometry were solved via partial differential equations obtained from the mass, momentum, and energy conservation equations under steady-state conditions, where no body force exists, as described below [20].

Continuity equation

$$\frac{\partial \bar{u}}{\partial x}+\frac{\partial \bar{v}}{\partial y}+\frac{\partial \bar{w}}{\partial z}=0. \tag{1}$$

Momentum equations

x momentum equation

$$\left[\bar{u}\frac{\partial \bar{u}}{\partial x}+\frac{\partial \overline{(u')^2}}{\partial x}\right]+\left[\bar{v}\frac{\partial \bar{u}}{\partial y}+\frac{\partial \overline{(u'v')}}{\partial y}\right]+\left[\bar{w}\frac{\partial \bar{u}}{\partial z}+\frac{\partial \overline{u'w'}}{\partial z}\right]=-\frac{1}{\rho}\frac{\partial \bar{p}}{\partial x}+v\left(\frac{\partial^2 \bar{u}}{\partial x^2}+\frac{\partial^2 \bar{u}}{\partial y^2}+\frac{\partial^2 \bar{u}}{\partial z^2}\right), \tag{2.1}$$

y momentum equation

$$\left[\bar{u}\frac{\partial \bar{v}}{\partial x}+\frac{\partial \overline{(v')^2}}{\partial x}\right]+\left[\bar{v}\frac{\partial \bar{v}}{\partial y}+\frac{\partial \overline{(v'v')}}{\partial y}\right]+\left[\bar{w}\frac{\partial \bar{v}}{\partial z}+\frac{\partial \overline{v'w'}}{\partial z}\right]=-\frac{1}{\rho}\frac{\partial \bar{p}}{\partial y}+v\left(\frac{\partial^2 \bar{v}}{\partial x^2}+\frac{\partial^2 \bar{v}}{\partial y^2}+\frac{\partial^2 \bar{v}}{\partial z^2}\right), \tag{2.2}$$

z momentum equation

$$\left[\bar{u}\frac{\partial \bar{w}}{\partial x}+\frac{\partial \overline{(w')^2}}{\partial x}\right]+\left[\bar{v}\frac{\partial \bar{w}}{\partial y}+\frac{\partial \overline{(w'v')}}{\partial y}\right]+\left[\bar{w}\frac{\partial \bar{w}}{\partial z}+\frac{\partial \overline{w'w'}}{\partial z}\right]=-\frac{1}{\rho}\frac{\partial \bar{p}}{\partial z}+v\left(\frac{\partial^2 \bar{w}}{\partial x^2}+\frac{\partial^2 \bar{w}}{\partial y^2}+\frac{\partial^2 \bar{w}}{\partial z^2}\right). \tag{2.3}$$

Energy equation

$$\left[\bar{u}\frac{\partial \bar{T}}{\partial x}+\bar{v}\frac{\partial \bar{T}}{\partial y}+\bar{w}\frac{\partial \bar{T}}{\partial z}\right]+\frac{\partial\overline{(u'T')}}{\partial x}+\frac{\partial\overline{(v'T')}}{\partial y}+\frac{\partial\overline{(w'T')}}{\partial z}=\frac{k}{\rho c_p}+v\left(\frac{\partial^2\bar{T}}{\partial x^2}+\frac{\partial^2\bar{T}}{\partial y^2}+\frac{\partial^2\bar{T}}{\partial z^2}\right). \quad (3)$$

Steady flow turbulence kinetic energy equation

$$\frac{\partial(\rho u k')}{\partial x}+\frac{\partial(\rho v k')}{\partial y}+\frac{\partial(\rho w k')}{\partial z}=\frac{\partial}{\partial x}\left(\frac{\mu_t}{\sigma_k}\frac{\partial k'}{\partial x}\right)+\frac{\partial}{\partial y}\left(\frac{\mu_t}{\sigma_k}\frac{\partial k'}{\partial y}\right)+\frac{\partial}{\partial z}\left(\frac{\mu_t}{\sigma_k}\frac{\partial k'}{\partial z}\right)+\mu_t\varphi-\rho\varepsilon. \quad (4)$$

Turbulence viscosity

$$\mu_t=C'_\mu\rho\frac{k'^2}{\varepsilon}. \quad (5)$$

In the k-ε turbulence model used in the work, ε indicates the turbulence distribution; $k'$and φ show the turbulence kinetic energy and the viscous dissipation term, respectively.

Turbulence kinetic energy

$$k'=\frac{1}{2}\left(\overline{u'^2}+\overline{v'^2}+\overline{w'^2}\right). \quad (6)$$

Viscous dissipation term

$$\varphi=2\mu\left[\left(\frac{\partial\bar{u}}{\partial x}\right)^2+\left(\frac{\partial\bar{v}}{\partial y}\right)^2+\left(\frac{\partial\bar{w}}{\partial z}\right)^2\right]+\mu\left[\left(\frac{\partial\bar{v}}{\partial x}+\frac{\partial\bar{u}}{\partial y}\right)^2+\left(\frac{\partial\bar{w}}{\partial y}+\frac{\partial\bar{v}}{\partial z}\right)^2+\left(\frac{\partial\bar{u}}{\partial z}+\frac{\partial\bar{w}}{\partial x}\right)^2\right]. \quad (7)$$

Turbulence kinetic energy disappearance equation

$$\begin{aligned}\frac{\partial(\rho\bar{u}\varepsilon)}{\partial x}+\frac{\partial(\rho\bar{v}\varepsilon)}{\partial y}+\frac{\partial(\rho\bar{w}\varepsilon)}{\partial z}&=\frac{\partial}{\partial x}\left(\frac{\mu_t}{\sigma_\varepsilon}\frac{\partial\varepsilon}{\partial x}\right)+\frac{\partial}{\partial y}\left(\frac{\mu_t}{\sigma_\varepsilon}\frac{\partial\varepsilon}{\partial y}\right)+\frac{\partial}{\partial z}\left(\frac{\mu_t}{\sigma_\varepsilon}\frac{\partial\varepsilon}{\partial z}\right)\\&+C_{1\varepsilon}\mu_t\frac{\varepsilon}{k'}\varphi-C_{2\varepsilon}\rho\frac{\varepsilon^2}{k'}.\end{aligned} \quad (8)$$

The model constants C_μ, $C_{1\varepsilon}$, $C_{2\varepsilon}$, σ_{k}, and σ_ε are the typical default values employed in the standard k-ε turbulence model [20]. The values of these constants were obtained via numerous iterations of data fitting for many turbulent flows: $C_\mu=0.09$, $C_{1\varepsilon}=1.44$, $C_{2\varepsilon}=1.92$, $\sigma_{\mathrm{k}}=1$, and $\sigma_\varepsilon=1.3$.

Re number was calculated as follows:

$$\mathrm{Re}=\frac{V_\infty D_h}{\nu}. \quad (9)$$

Hydraulic diameter

$$D_h=\frac{4A_c}{P}=\frac{4(2h)(4h)}{2(2h+4h)}=\frac{4h}{3}. \quad (10)$$

Nu number is taken as the ratio of the conduction heat transfer rate to the convection heat transfer rate:

$$-k\left(\frac{\partial T}{\partial n}\right)_s=h(T_\infty-T_s)\ \text{ and }\ \mathrm{Nu}=\frac{hL}{k}. \quad (11)$$

Here, n is the direction perpendicular to the surface and the local Nu number is calculated as above.

The mean heat transfer coefficient:

$$h_m = \frac{1}{L} h d_x. \tag{12}$$

The mean Nu number:

$$\mathrm{Nu}_m = \frac{h_m L}{k}. \tag{13}$$

The pressure drop:

$$\Delta p = f \frac{L}{D_h} \frac{\rho V^2}{2}. \tag{14}$$

Here $L = 20h$ is the length of the channel section with a constant surface temperature.

3. GEOMETRIC MODEL

Figure 1a shows the flat (without chamfer) geometric structure of the backward-facing step model, while Fig. 1b presents the step corner structures with an h/2- and h-long chamfer. As shown in Fig. 1, the length of the heated section is 20h and h is equal to 0.05 m. The expansion rate of the backward-facing step, which is the ratio of the lateral lengths (3h) at the end of the channel and in the part where the fluids enter the channel (2h), is 1.5. The chamfer lengths taken for the corners are h/2 and h. The fluids are distilled water (DW), 0.01% vol. GO-DW, and 0.02% vol. GO-DW nanofluids. The channel inlet velocities of the fluids (V_∞) are 0.0806 m/s, 0.13535 m/s, and 0.1064 m/s for DW, 0.01% vol. GO-DW, and 0.02% vol. GO-DW, respectively, at Re = 5000. While the channel inlet fluid temperature is 303 K, the wall surface temperature behind the backward-facing step is 316.5 K. The experimental thermophysical values of the DW and GO-DW nanofluids with volumetric concentrations of 0.01% and

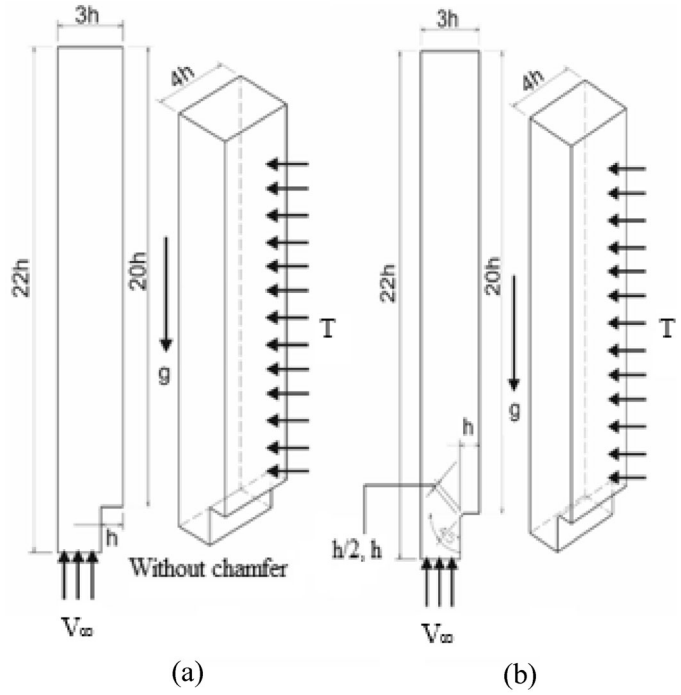

Fig. 1. Backward-facing step models. (a) Without chamfer; (b) h/2- and h-long chamfer.

0.02% are as follows: $\rho = 995.8$ kg/m^3, $c_p = 4178.4$ J/kgK, k = 0.6172 W/mK, $\mu = 0.0008034$ N s/m^2, $\rho = 996.1$ kg/m^3, $c_p = 4178.4$ J/kgK, k = 0.6696 W/mK, $\mu = 0.001$ N s/m^2 [21], $\rho = 996.1$ kg/m^3, $c_p = 4178.4$ J/kgK, k = 0.678 W/mK, $\mu = 0.001060$ N s/m^2 [22].

This study was carried out under the following assumptions

(a) The flow field for the backward-facing step flow was three-dimensional, steady, and turbulent.

(b) The calculations were done for an incompressible flow.

(c) DW and the GO-DW nanofluids with volumetric concentrations of 0.01% and 0.02% were used as working fluids.

(d) 316.5 K as a constant surface temperature was applied to the wall surface behind the backward-facing step, while the other walls were adiabatic.

(e) The thermal properties of the fluids were constant.

(f) There was no heat generation for both fluids and walls.

4. RESULTS AND EVALUATION

Figure 2 presents comparison of the presented work and a numerical study performed by Togun et al. [23] for a backward-facing step model with an inlet length of 1.25 cm, expansion rate of 2, upstream length of 200 cm, and heated (4000 W/m^2) downstream length of 150 cm for DW at Re = 10000. The results were found to be in good agreement. It is concluded that the results of this study are reasonable and acceptable.

In order to determine the impact of the mesh number on the mean Nu number Nu_m and velocity V_m, we carried out mesh independence tests for Re = 5000, using water as a fluid in a backward-facing step flow channel without chamfer (Table 1). According to the tests, 988942 mesh elements are sufficient for a channel without chamfer. In addition, Table 2 presents the number of mesh elements used in the backward-facing step flow channels without chamfer and with the chamfers h/2 and h long.

Figure 3 shows the Nu number variations along the channels with backward facing steps without chamfer and with the chamfers h/2 and h long at Re numbers of 7500 and 10000 for DW and the GO-DW nanofluids with volumetric concentrations of 0.01% and 0.02%. For the nanofluids (0.01% GO-DW and 0.02% GO-DW) and DW, up to 0.28 m of the channel section, which is a separated flow region of the backward-facing step, the channel with the chamfer h long has a Nu number higher than that of the channels with the chamfer h/2 long and without chamfer. After this channel length, as seen

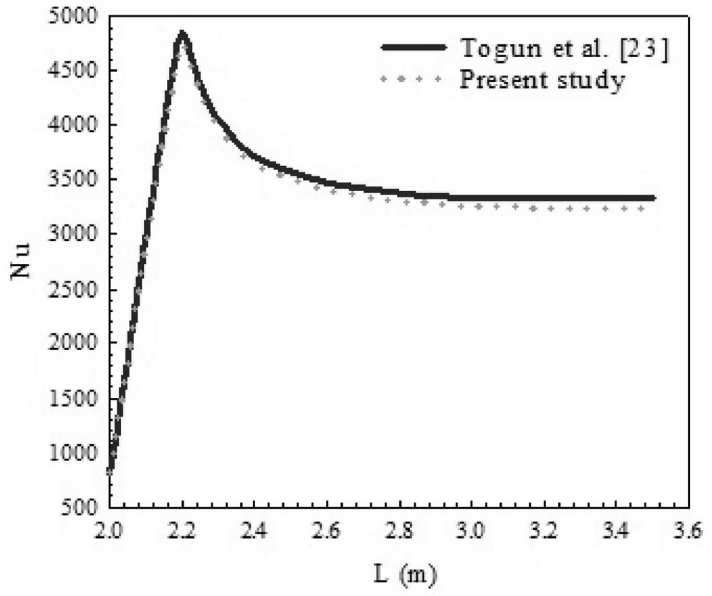

Fig. 2. Comparison of results of presented study with those by Togun et al. [23].

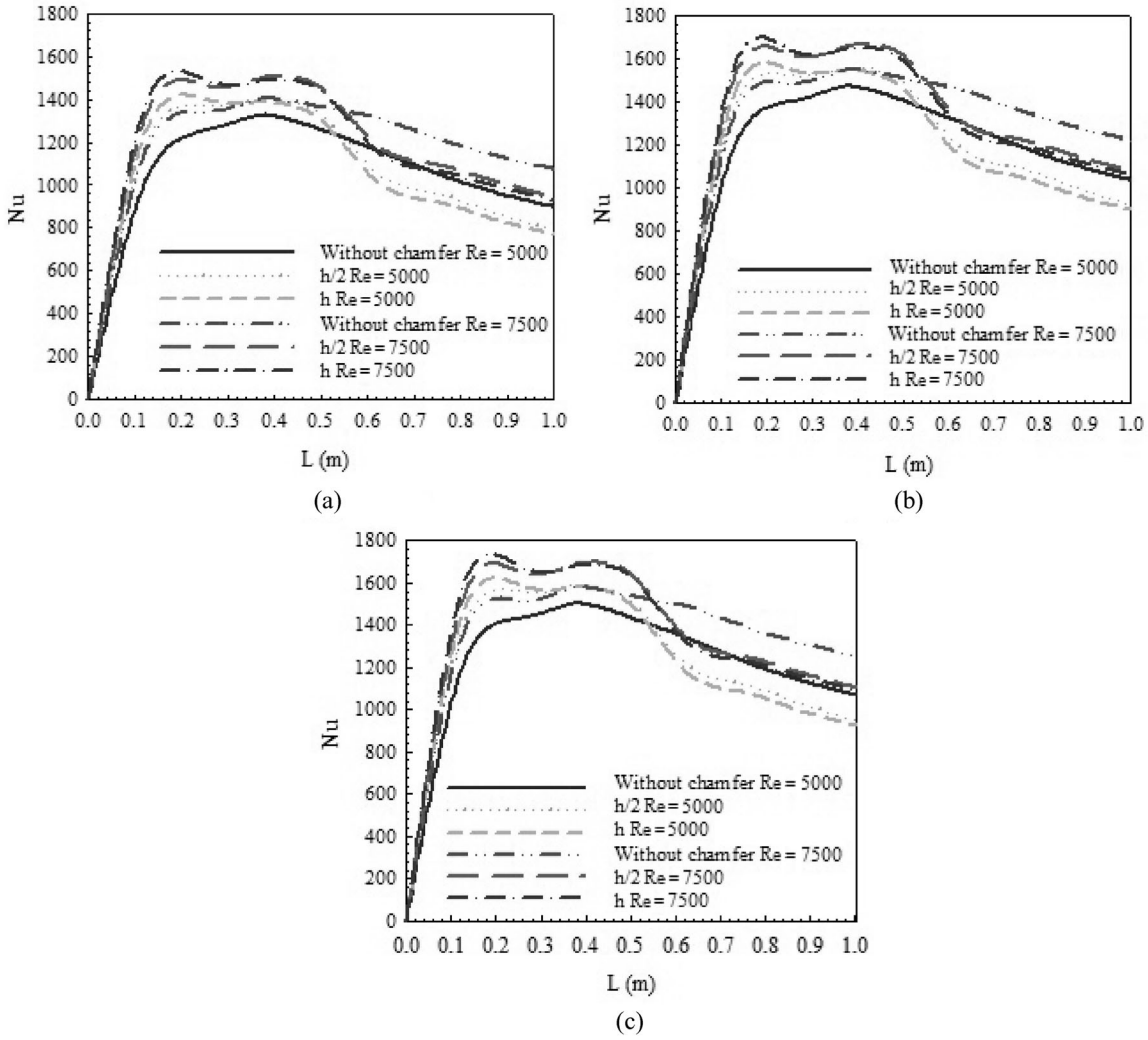

Fig. 3. Nu number variation. (a) DW; (b) 0.01% GO-DW; (c) 0.02% GO-DW.

Table 1. Mesh test results for Nu_m and V_m in channel without chamfer

Mesh number	Nu_m	V_m (m/s)
939495	1185.25	0.034254
988942	1196.56	0.034824
1080420	1196.48	0.034471

from Fig. 3, the Nu number is larger for the channel with the h/2-long chamfer, where the flow mixing is better. However, after the reunification region, the Nu number values of the fluids with temperature enhanced due to the heat transfer in the separated flow section beginning from the 0.56 m channel length are lower than those of the channel without chamfer for both DW and the nanofluids (Fig. 3). The Nu number values increase with the Re number. According to this, it is observed that for the 0.01% GO-DW and 0.02% GO-DW nanofluids, the mean Nu number of the backward-facing step geometry with the chamfer length h exceeds by 11.7% and 14.33%, respectively, that of DW at Re = 7500. So, besides

Table 2. Mesh numbers in channels without chamfer and with h/2- and h-long chamfer

Channel type	Mesh number
Without chamfer	988942
h/2	988594
h	991830

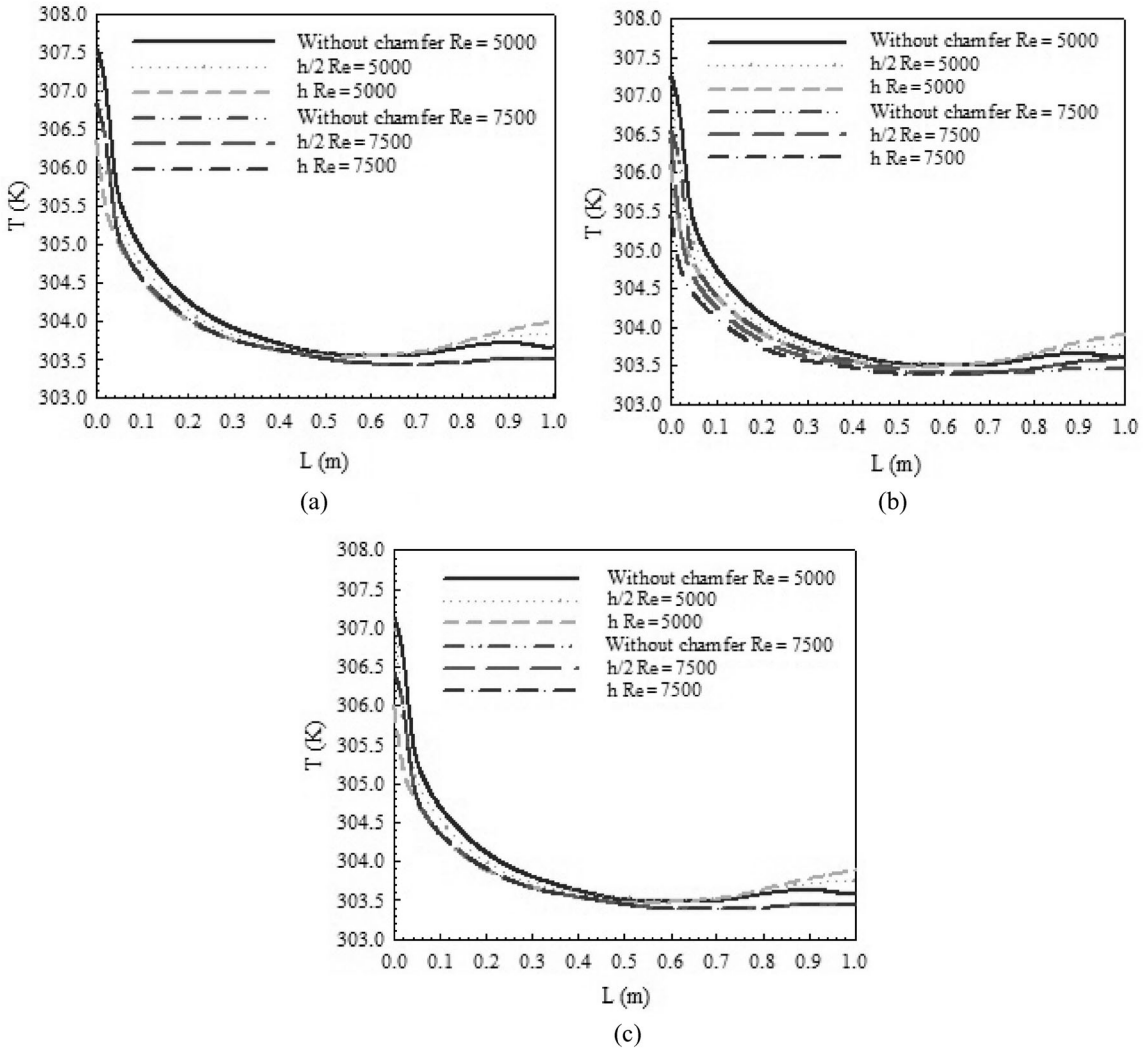

Fig. 4. Fluid temperature variation. (a) DW; (b) 0.01% GO-DW; (c) 0.02% GO-DW.

the chamfer given to the corner section in geometry, the use of nanofluid, especially in backward step flow applications with flow separation, increases the heat transfer.

Figure 4 presents temperature variations throughout a 0.5h length, which is half the height of the channel step, in the backward-facing step flow geometries without chamfer and with the chamfer h and h/2 long for DW, 0.01% GO-DW, and 0.02% GO-DW fluids for different Re numbers. According to the graphs, in the backward-facing step channels, the minimum fluid temperature is obtained for the 0.02% GO-DW nanofluid, whereas the maximum temperature value is reached for DW. However, as in the Nu number graphs in Fig. 3, up to a channel length of approximately 0.28 m, the fluid temperature is lower with a chamfer and the heat transfer is better in the channel with the h-long chamfer. However, for Re =

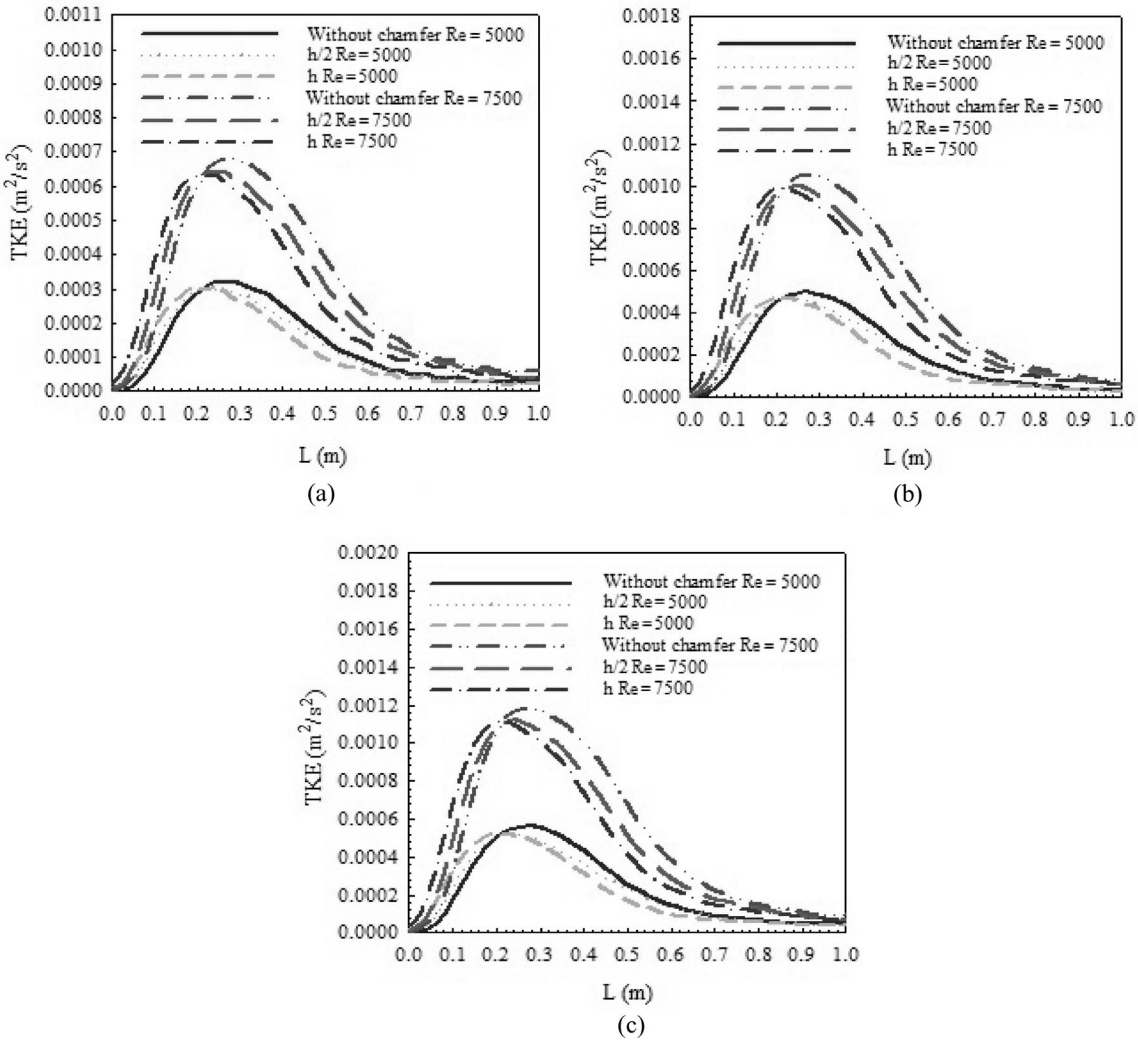

Fig. 5. TKE variation. (a) DW; (b) 0.01% GO-DW; (c) 0.02% GO-DW.

5000, the fluid temperatures increase after this section of the channel and especially towards the channel exit; with the chamfers h and h/2 long, the fluid temperatures are higher than those without chamfer.

Figure 5 presents the turbulence kinetic energy (TKE) variations of the DW, 0.01% GO-DW, and 0.02% GO-DW fluids at different Re numbers for the 0.5h channel step height. A higher turbulence kinetic energy means better mixing of the fluid. Therefore, higher TKE values are obtained for all the channels with chamfers and all fluid types at Re number equal to 7500. Besides, while for the backward-facing step geometry with the h-long chamfer, the TKE values are higher in the inlet section of the channels, which is the separated flow region, the TKE values of the channels without chamfer and with the chamfer h/2 long begin to increase in the last section of the channels. However, the highest fluid mixing value (TKE) is achieved in the GO-DW nanofluid with a volumetric concentration of %0.02.

Figure 6 presents pressure variations throughout the 0.5h step height for different Re numbers for DW and the GO-DW (0.01% vol. and 0.02% vol.) nanofluids for the channels with the chamfers h and h/2 long and without chamfer. In parallel with the TKE changes in Fig. 5, higher pressure variation values are obtained for the nanofluids, where the fluid mixing is better, but the pressure values achieved for distilled water (DW) are lower (Fig. 6c). In addition, especially at Re = 7500, it can be seen from Figs. 6a and 6b that very close values are obtained without chamfer due to the fact that the nanofluids (0.01% vol. GO-DW and 0.02% vol. GO-DW) direct towards the backward-facing step part of the channel, which provides better mixing.

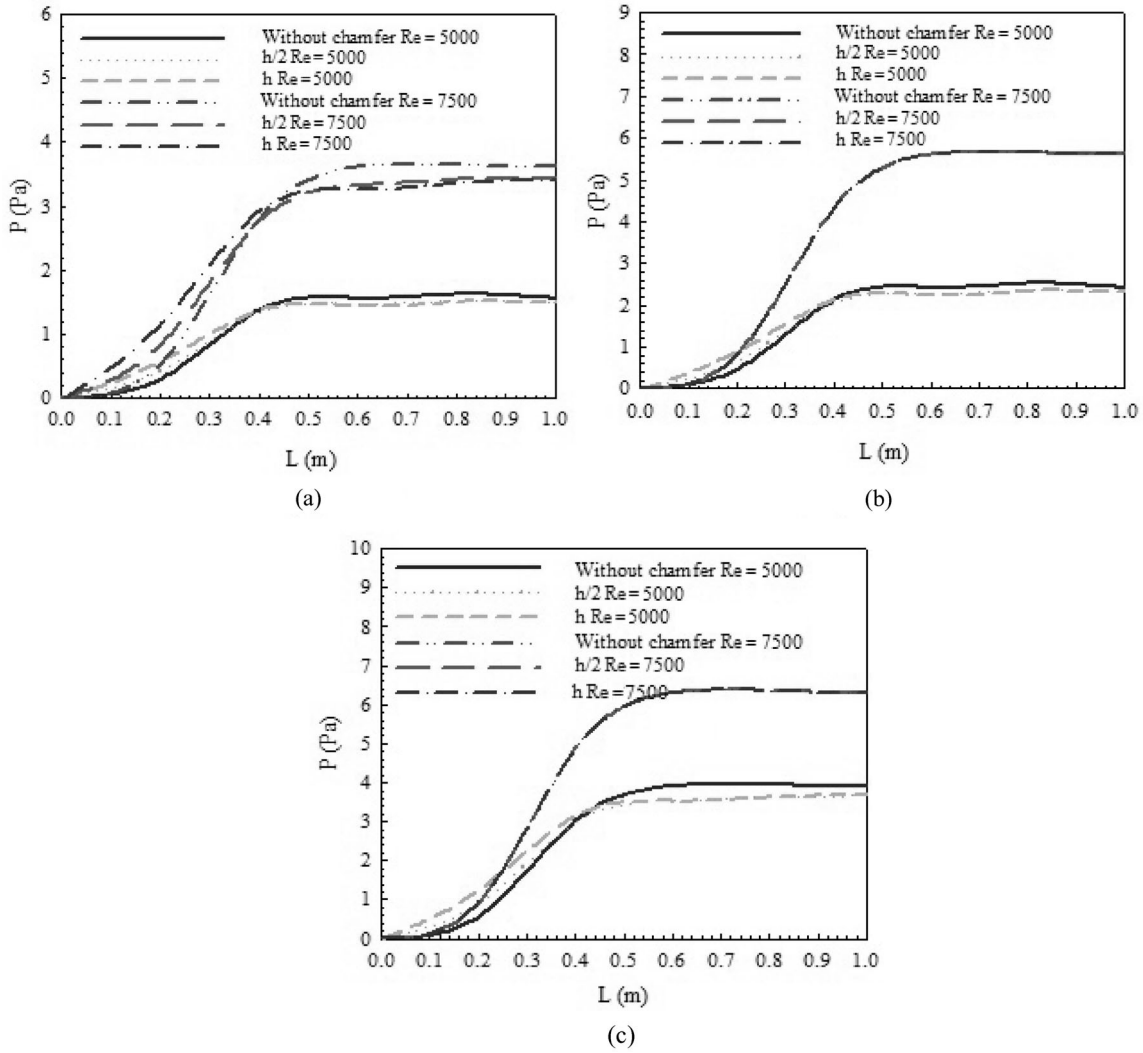

Fig. 6. Pressure variation. (a) DW; (b) 0.01% GO-DW; (c) 0.02% GO-DW.

Figures 7, 8, and 9 present the velocity distribution contours of the channels without chamfer and with the chamfers h/2 and h long for DW, 0.01% GO-DW, and 0.02% GO-DW at a Re number of 5000 (7A-8A-9A) and 7500 (7B-8B-9B). The red color at the channel inlet, which indicates a high speed fluid, changes to the blue color due to the speed decrease in the backward-facing step sections. However, when the channel has a chamfer, the flow is accelerated because the fluid directs toward the backward-facing step, and so the color of the flow becomes light blue in this region. Besides, the change of the dark blue color of the flow to the light blue one, especially in the separated flow region of the backward-facing step section of the channel with the h-long chamfer, can be considered as indication that the flow moves better in this part. It can be seen from the maximum values in the velocity distribution contour, where the fluid velocity reaches the highest values for both Re = 5000 and Re = 7500 for the 0.02% GO-DW nanofluid.

Figures 10, 11, and 12 present the temperature distribution contours of DW and the 0.01% GO-DW and 0.02% GO-DW nanofluids for the straight model (without chamfer) and models of the backward-facing step with the chamfers h/2 and h long at Re numbers of 5000 (10A-11A-12A) and 7500 (10b-11b-12b). As can be seen from the temperature contour distributions for all the fluids, since the mobility of the fluid in the backward step section is less in the flat model without chamfer, stronger warming occurs as compared with the chamfered models. Therefore, the temperature in this part is lighter blue (Fig. 10A-B (a), Fig. 11A-B (a), and Fig. 12A-B (a)). However, when the channel is chamfered, since

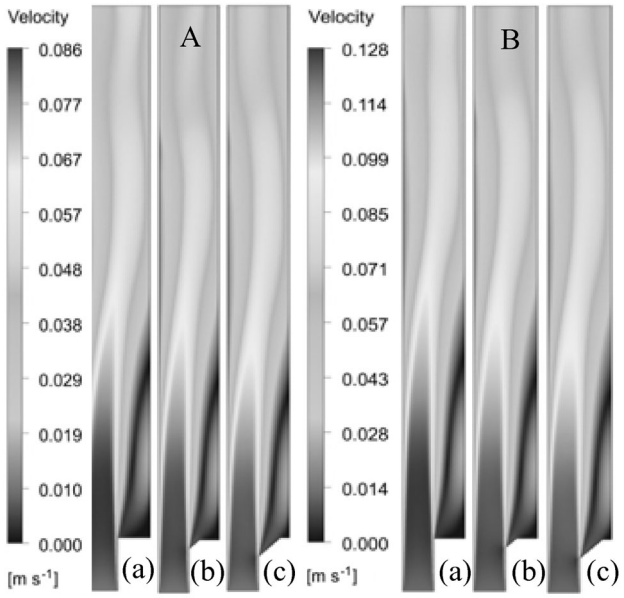

Fig. 7. Velocity distribution contours for DW. A: Re = 5000; B: Re = 7500. (a) Without chamfer; (b) h/2-long chamfer; (c) h-long chamfer.

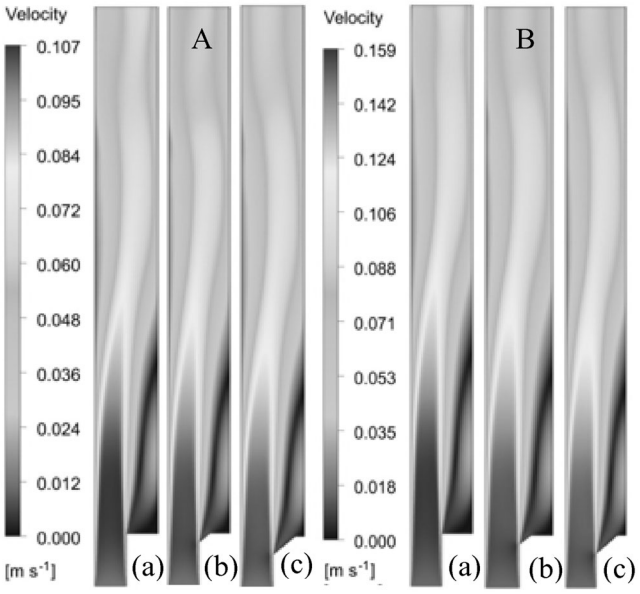

Fig. 8. Velocity distribution contours for 0.01% GO-DW. A: Re = 5000; B: Re = 7500. (a) without chamfer; (b) h/2-long chamfer; (c) h-long chamfer.

in the duct with the h-long chamfer the flow mobility increases in the separated flow region towards the backward-facing step, the temperature change spreads to the flow of the entire channel, shrinking the light blue part of the corner part. Thus, the heat transfer in the channel grows. In addition, it can be seen that, especially in the ducts with the 0.02% GO-DW nanofluid at Re = 7500, there is a greater increase in the heat transfer due to the chamfer in the channel.

Figures 13, 14, and 15 visualize the streamline distributions for DW and the nanofluids 0.01% GO-DW and 0.02% GO-DW at Re = 5000 (A) and Re = 7500 (B) in the channels without chamfer and with the chamfer h/2 and h long, respectively. The determination of the length of the reattachment

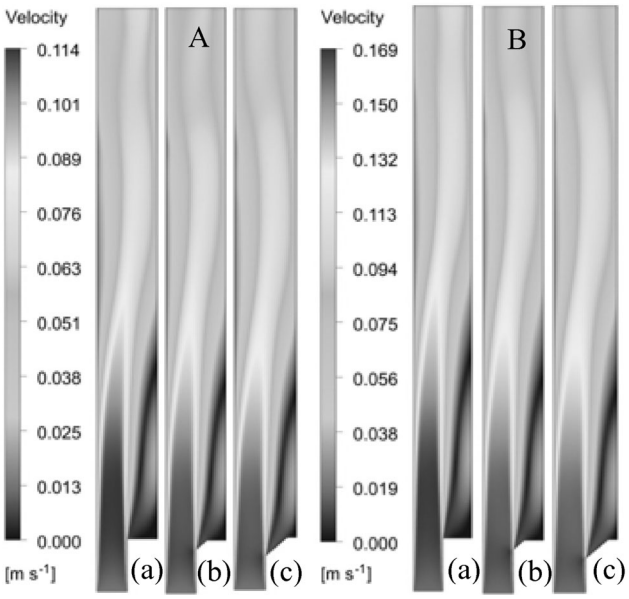

Fig. 9. Velocity distribution contours for 0.02% GO-DW. A: Re = 5000; B: Re = 7500. (a) without chamfer; (b) h/2-long chamfer; (c) h-long chamfer.

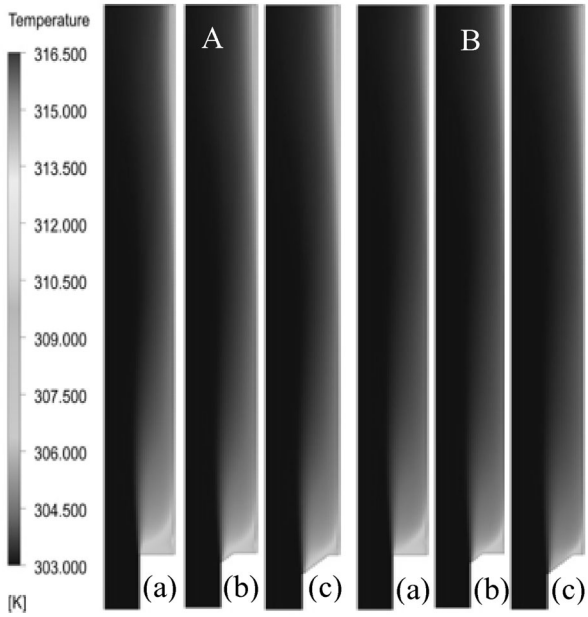

Fig. 10. Temperature distribution contours for DW. A: Re = 5000; B: Re = 7500. (a) without chamfer; (b) h/2-long chamfer; (c) h-long chamfer.

point provides an idea about the mobility of the flow in the channels with a chamfered backward-facing step. For this purpose, the vertical coordinates of the center point are determined on the streamline distributions. As seen from the figures, in the chamfered channels, the center point coordinates are back than those in the model without chamfer. Therefore, the vertical length of the center point is smaller. This situation shows us that the flow moves to the backward-facing step. However, the model with the h-long chamfer has the shortest center point line. Thus, the fluid motion in the separated flow section in the channel having the h-long chamfer h is further improved as compared with the channels with

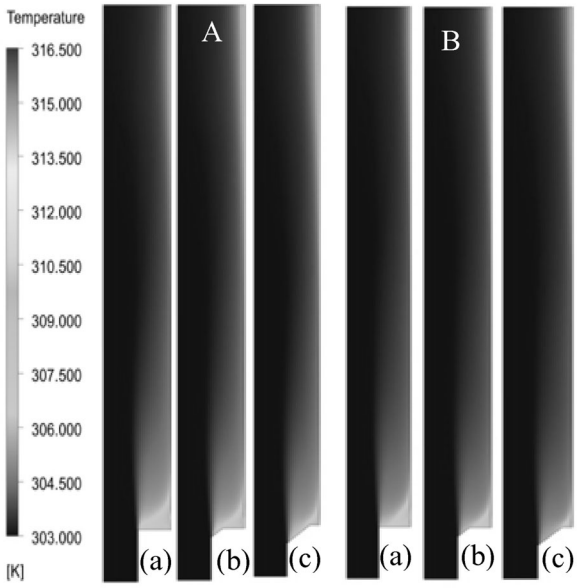

Fig. 11. Temperature distribution contours for 0.01% GO-DW. A: Re = 5000; B: Re = 7500. (a) without chamfer; (b) h/2-long chamfer; (c) h-long chamfer.

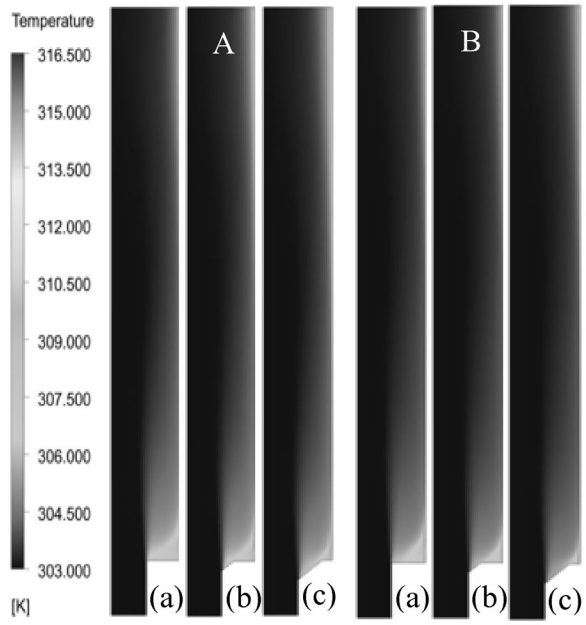

Fig. 12. Temperature distribution contours for 0.02% GO-DW. A: Re = 5000; B: Re = 7500. (a) without chamfer; (b) h/2-long chamfer; (c) h-long chamfer.

the h/2-long chamfer and without chamfer. In addition, at Re = 7500, the center point distances of the streamline are decreased for both nanofluids and distilled water, although they are very close.

5. CONCLUSIONS AND ASSESSMENTS

A backward-facing step flow is encountered in many devices such as collectors of power conversion systems and internal and external flows of heat storage containers and is considered as an important geometric model due to the complex structure of the flow. The conclusions drawn from the results of this study can be summarized as follows:

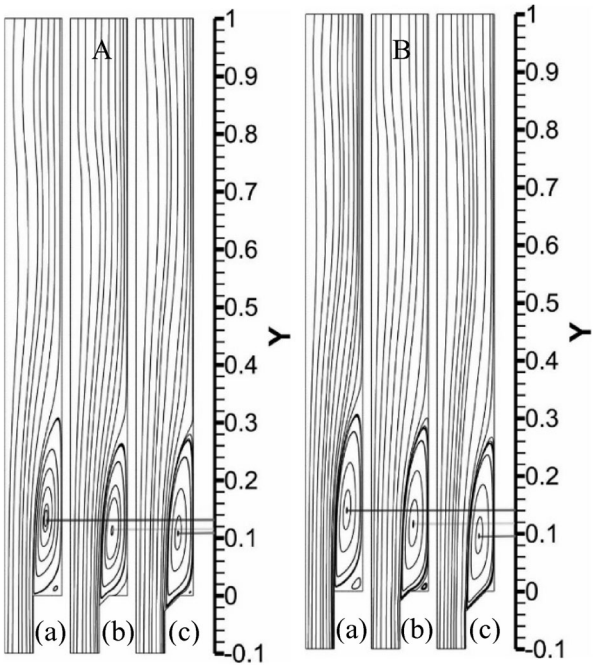

Fig. 13. Streamline distributions for DW. A: Re = 5000; B: Re = 7500. (a) without chamfer; (b) h/2-long chamfer; (c) h-long chamfer.

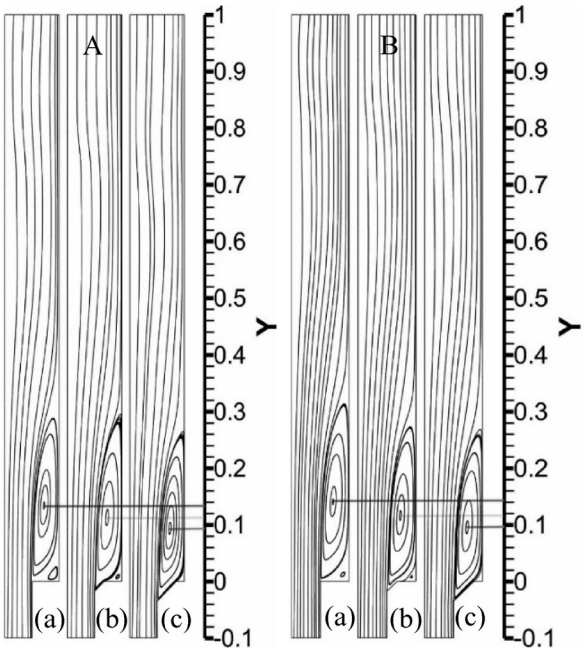

Fig. 14. Streamline distributions for 0.01% GO-DW. A: Re = 5000; B: Re = 7500. (a) without chamfer; (b) h/2-long chamfer; (c) h-long chamfer.

—For Re = 7500, for the 0.01% vol. GO-DW and 0.02% vol. GO-DW nanofluids, the mean Nu number of the backward-facing step geometry with the h-long chamfer exceeds by 11.7% and 14.33%, respectively, that of DW.

—When the temperature variations are examined, the lowest fluid temperature is obtained for the GO-DW nanofluid with the volumetric concentration of 0.02%, while the highest temperature value

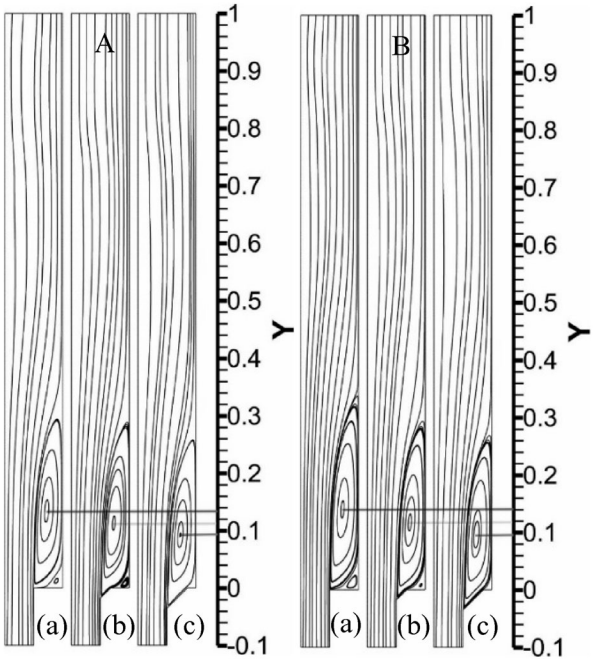

Fig. 15. Streamline distributions for 0.02% GO-DW. A: Re = 5000; B: Re = 7500. (a) without chamfer (b); h/2-long chamfer; (c) h-long chamfer.

is achieved in the backward-facing step flow model with distilled water. However, while the fluid temperature for the h-long chamfer is lower as compared with other models in the separated flow region due to the better heat transfer, for Re = 5000 the fluid temperatures for the h- and h/2-long chamfers are higher than that of the channel without chamfer towards the end of the channel along with the recombination of the flow.

—While a higher TKE value is obtained in the inlet part of the duct for the backward-facing step flow model with the h-long chamfer, the reached TKE values for the h/2-long chamfer channel show a larger increase in the farther parts of the channels. Towards the end of the channel, especially for Re = 7500, the TKE values of the chamfered channels are higher than those of the channel without chamfer. However, the highest fluid mixing value (TKE) is achieved with the 0.02% GO-DW nanofluid.

—Higher pressure variation values are obtained for the nanofluids with better mixing, but the pressure values achieved for distilled water are lower. Besides, very close values are obtained for the chamfered channels as compared with the channel without chamfer, which is a result of better mixing of the flow for the nanofluids, especially at Re = 7500. For distilled water, the pressure values of the chamfered ducts are lower than those of the channel without chamfer.

—As can be seen from the velocity contour distributions, the turning of the dark blue colored part of the flow towards the light blue in the separated flow zone for the backward-facing step section for the h-long chamfer channel can be considered as an indicator of the fact that the flow moves better in this part. However, the fluid velocity reaches the highest values for both Re = 5000 and Re = 7500 for the 0.02% GO-DW nanofluid.

—When looking at the temperature contour distributions, one can see that the chamfered models are less warm since the mobility of the fluid is less in the backward-facing step section of the channel without chamfer. Therefore, this part is lighter blue. However, the light blue colored part in the corner section of the channel with the h-long chamfer in the separated flow region decreases towards the backward-facing step and the temperature change spreads to the flow of the entire channel.

—The center point coordinates in the chamfered channels for fluids are back as compared with the channel without chamfer, so the vertical length of the center point is smaller. This is an indication that the flow gets into motion towards the backward-facing step.

—As a result, it is necessary to make duct designs that will reduce the separated flow zone in order to increase the heat transfer. In addition, selection of fluids with high heat transfer coefficients such as nanofluids is extremely important in applications where a larger amount of heat transfer is desired.

NOTATIONS

A_c—inlet cross-sectional area (m^2)

D_h—hydraulic diameter (m)

f—friction factor

h—local convection heat transfer coefficient ($W/m^2 \cdot K$)

k—thermal conductivity coefficient ($W/m \cdot K$)

L—channel length (m)

V—fluid velocity in the channel entry (m/s)

c_p—specific heat ($J/kg \cdot K$)

P—perimeter of the tube (m)

P—pressure (Pa)

Δp—pressure drop (Pa)

$\bar{T}$—mean temperature (K)

$\bar{u'}$, $\bar{v'}$, $\bar{w'}$—mean fluctuating velocity components in the x, y, z directions (m/s)

$\bar{u}$, $\bar{v}$, $\bar{w}$—mean velocity components in the x, y, z directions (m/s)

Re—Reynolds number

Nu—Nusselt number

k'—turbulence kinetic energy (m^2/s^2)

Greek Letters

υ—kinematic viscosity (m^2/s)

ρ—density (kg/m^3)

μ—dynamic viscosity ($kg/s \cdot m$)

μ_t—turbulence viscosity ($kg/s \cdot m$)

φ—viscous dissipation term (m^2/s^3)

ε—turbulence dissipation rate (m^2/s^3)

Subscripts

s—surface

∞—fluid

m—mean

FUNDING

This work was supported by the Scientific Research Project Fund of Sivas Cumhuriyet University under project no. SMYO-026.

REFERENCES

1. Trisaksri, V. and Wongwises, S., Critical Review of Heat Transfer Characteristics of Nanofluids, *Ren. Sust. Energy Rev.*, 2007, vol. 11, pp. 512–523.
2. Maxwell, J.C., *A Treatise on Electricity and Magnetism*, 2nd ed., Cambridge, England: Oxford Clarendon Press, 1904.
3. Gupte, S.K., Advani, S.G., and Huq, P., Role of Micro-Convection due to Non-Affine Motion of Particles in a Mono-Disperse Suspension, *Int. J. Heat Mass Transfer*, 1995, vol. 38, pp. 2945–2958.
4. Kim, S.J., Bang, I.J., Buongiorno, J., and Hu, L.W., Surface Wettability Change during Pool Boiling of Nanofluids and Its Effect on Critical Heat Flux, *Int. J. Heat Mass Transfer*, 2007, vol. 50, pp. 4105–4116.
5. Kwark, S.M., Kumar, R., Moreno, G., Yoo, J., and You, S.M., Pool Boiling Characteristics of Low Concentration Nanofluids, *Int. J. Heat Mass Transfer*, 2010, vol. 53, pp. 972–981.
6. Hong, K.S., Hong, T.K., and Yang, H.S., Thermal Conductivity of Fe Nanofluids Depending on the Cluster Size of Nanoparticles, *Appl. Phys. Lett.*, 2006, vol. 88, pp. 1–3.
7. Hwan, L., Hwang, K., Janga, S., Lee, B., Kim, J., Choi, S.U.S., and Choi, C., Effective Viscosities and Thermal Conductivities of Aqueous Nanofluids Containing Low Volume Concentrations of Al_2O_3 Nanoparticles, *Int. J. Heat Mass Transfer*, 2008, vol. 51, pp. 2651–2656.
8. Xie, H., Lee, H., Youn, W., and Choi, M., Nanofluids Containing Multiwalled Carbon Nanotubes and Their Enhanced Thermal Conductivities, *J. Appl. Phys.*, 2003, vol. 94, pp. 4967–4971.
9. Novoselov, K., Geim, A.K., Morozov, S., Jiang, D., Grigorieva, I.V., Dubonos, S., and Firsov, A., Two-Dimensional Gas of Massless Dirac Fermions in Graphene, *Nature*, 2005, vol. 438, pp. 197–200.
10. Balandin, A.A., Ghosh, S., Bao, W., Calizo, I., Teweldebrhan, D., Miao, F., and Lau, C.N., Superior Thermal Conductivity of Single-Layer Graphene, *Nano Lett.*, 2008, vol. 8, pp. 902–907.
11. Yu, W., Xie, H., Chen, L., and Li, Y., Enhancement of Thermal Conductivity of Kerosene-Based Fe_3O_4 Nanofluids Prepared via Phase-Transfer Method, *Colloids Surfaces A*, 2010, vol. 355, pp. 109–113.
12. Armaly, B.F., Durst, F., Pereira, J.C.F., and Schönung, B., Experimental and Theoretical Investigation of Backward-Facing Step Flow, *J. Fluid Mech.*, 1983, vol. 127, pp. 473–496.
13. Nadge, P. and Govardhan, R., High Reynolds Number Flow over a Backward-Facing Step: Structure of the Mean Separation Bubble, *Exp. Fluids*, 2014, vol. 55, pp. 1–22.
14. Kasagi, N. and Matsunaga, A., Three-Dimensional Particle-Tracking Velocimetry Measurement of Turbulence Statistics and Energy Budget in a Backward-Facing Step Flow, *Int. J. Heat Fluid Flow*, 1995, vol. 16, pp. 477–485.
15. Le, H., Moin, P., and Kim, J., Direct Numerical Simulation of Turbulent Flow over a Backward-Facing Step, *J. Fluid Mech.*, 1997, vol. 330, pp. 349–374.
16. Simpson, R.L., Turbulent Boundary-Layer Separation, *Annu. Rev. Fluid Mech.*, 1989, vol. 21, pp. 205–232.
17. Vogel, J.C. and Eaton, J.K., Combined Heat Transfer and Fluid Dynamic Measurements Downstream of a Backward-Facing Step, *J. Heat Transfer*, 1985, vol. 107, pp. 922–929.
18. Keating, A., Piomelli, U., Bremhorst, K., and Nei, S., Large-Eddy Simulation of Heat Transfer Downstream of a Backward-Facing Step, *J. Turbul.*, 2004, vol. 5, pp. 1–27.
19. Avancha, R.V. and Pletcher, R.H., Large Eddy Simulation of the Turbulent Flow Past a Backward-Facing Step with Heat Transfer and Property Variations, *Int. J. Heat Fluid Flow*, 2002, vol. 23, pp. 601–614.
20. *ANSYS Inc., ANSYS FLUENT User's Guide, Fluent,* Netherland, Lebanon: ANSYS Press, 2003.
21. Karabulut, K., Buyruk, E., and Kılınc, F., Experimental Investigation of the Effect of Graphene Oxide (GO)-Distilled Water Nanofluid Usage on Heat Transfer Increment in Circular Tubes Having Different Diameters, *Int. J. Eng. Res. Dev.*, 2019, vol. 11, pp. 282–301.
22. Karabulut, K., Buyruk, E., and Kılınc, F., Experimental Investigation of the Effect of Nanofluid Including Graphene-Oxide Nanoparticles on Convective Heat Transfer and Pressure Drop Enhancement in a Straight Pipe, *Engin. Machin.*, 2018, vol. 59, pp. 45–67.
23. Togun, H., Safaei, M.R., Sadri, R., Kazi, S.N., Badarudin, A., Hooman, K., and Sadeghinezhad, E., Numerical Simulation of Laminar to Turbulent Nanofluid Flow and Heat Transfer over a Backward-Facing Step, *Appl. Math. Comp.*, 2014, vol. 239, pp. 153–170.